ORIGINAL ARTICLE

Revisiting Doppler positioning performance with LEO satellites

Chuang Shi[1,2,3] · Yulu Zhang[1,2] · Zhen Li[2,3]

Abstract

Recently, the Doppler shifts from Low Earth Orbit (LEO) satellites have been used to augment GNSS and provide navigation services. We propose a Doppler-only point-solution algorithm for GNSS-like navigation systems operated in LEO. The proposed algorithm can simultaneously estimate the receiver clock drift, position and velocity. Then, we analyze the main error sources in Doppler positioning. To achieve the meter-level positioning accuracy, the satellite position and velocity errors should be within several meters and several centimeters per second, respectively. The ionospheric delay rates of C-band signal will cause about 1 m error in Doppler positioning, which can be eliminated using the ionosphere-free combination. The Doppler positioning accuracy will deteriorate sharply by dozens of meters if there are no corrections for the tropospheric errors. Subsequently, we analyze the Doppler positioning performance. The undifferenced Doppler positioning accuracy is at meter level, which is comparable with the pseudorange-based positioning in GNSS. To ensure convergence in the LEO-based Doppler positioning, the initial receiver position error should be less than 300 km when the satellites orbit is at an altitude of 550 km.

Keywords Doppler positioning · Low Earth Orbit (LEO) · Range rate · Doppler dilution of precision (DDOP)

Introduction

Recently, Low Earth Orbit (LEO) communication constellations such as Starlink and OneWeb have rapidly developed. These broadband internet providers plan to deploy thousands of satellites into their constellations. Compared with Global Navigation Satellite System (GNSS) satellites in Medium Earth Orbit, LEO satellites have advantages in received signal strength, rapid change of geometry in ranging and large Doppler shift in received frequency (Reid et al. 2018). These desirable attributes would be useful in GNSS-challengeable places like urban canyons and indoors. Therefore, LEO constellations have been considered a promising alternative positioning, navigation and timing (PNT) resource.

Existing applications of LEO satellites in navigation are mainly in two aspects, i.e., augmenting GNSS or providing PNT services independently. In the aspect of GNSS augmentation, LEO satellites can enhance the orbit determination for GNSS satellites with their onboard GNSS observations (Zhao et al. 2017; Zeng et al. 2018) and broadcast navigation augmentation information (Meng et al. 2018). Besides, Joerger et al. (2010) and Li et al. (2019) proposed some combined GNSS/LEO observation models to improve convergence performance for precise point positioning (PPP).

There are mainly two methods to provide standalone PNT services with LEO satellites. One is to design new navigation signals and payloads to support navigation capabilities. For example, research groups in the Satelles company and Iridium NEXT designed a Satellite Time and Location (STL) signal to provide PNT services (Lawrence et al. 2016). Reid et al. (2016) studied the approaches of leveraging LEO constellations for navigation. Their results indicate that using the LEO constellation for navigation is feasible. The other is to exploit LEO satellites in opportunistic navigation frameworks. The first issue to be addressed is how to estimate the states (position, velocity and clock drift) of the satellite and receiver simultaneously, as the orbital elements of LEO satellites are not known precisely. Ardito et al.

✉ Zhen Li
  hpulizhen@163.com

1 School of Electronic and Information Engineering, Beihang University, 37 Xueyuan Road, Beijing 100191, China

2 Key Laboratory of Navigation and Communication Fusion Technology, Ministry of Industry and Information Technology, 37 Xueyuan Road, Beijing 100191, China

3 Research Institute for Frontier Science, Beihang University, 37 Xueyuan Road, Beijing 100191, China

(2019) solved this problem using a simultaneous tracking and navigation framework. Khalife et al. (2020) proposed a differential framework to deal with this problem. The other challenge is to extract navigation observables from the LEO satellite signals. Farhangian and Landry (2020), Khalife and Kassas (2019a, 2019b) and Orabi et al. (2021) designed specialized receivers to obtain the pseudorange, carrier phase and Doppler measurements. Among them, the Doppler shift is generally easy to measure from these modulated signals (Khalife et al. 2021; Psiaki and Slosman 2019). The feasibility is the main advantage of Doppler measurements, especially for LEO communication satellites. Besides, the Doppler measurement is less affected by multipath effects than pseudorange. The Doppler shifts can also be used for velocity estimation (Chen et al. 2013), orbit and attitude determination (Jayles et al. 2010; Park et al. 2011). Thus, the Doppler shift observations have attracted much attention in LEO-based navigation.

In LEO-based Doppler positioning, the pioneering early TRANSIT navigation system is the first satellite-based Doppler positioning system (Kershner and Newton 1962). This system was introduced for military applications in 1964 and then was released for public use to provide positioning and navigation service in 1968 (Kouba 1983). It had more than 10 satellites in polar orbits at an altitude of about 1100 km. Typically one receiver could observe only one satellite at a time. The point positioning accuracy was around 100–200 m using about 2 min of Doppler shift observations. The positioning accuracy can be further improved with ionospheric delay corrected by dual-frequency (150 MHz and 400 MHz). For stationary receivers, the sub-meter positioning accuracy could be achieved using the precise ephemeris determined by the US Defense Mapping Agency and observations over a period of several days with 30 or more satellite passes (Kouba 1983). The relative position of simultaneously observing stations separated by distances up to 250 km could be computed with an accuracy of better than 40 cm at eight-hour intervals (Anderle 1979). With the advent of the Global Positioning System (GPS) and its superior performance, the TRANSIT was decommissioned in 1996.

In recent years, Benzerrouk et al. (2019), Tan et al. (2019) and Neinavaie et al. (2021) have explored the approaches of Doppler positioning using LEO constellations. The positions and velocities of LEO satellites are computed from the Two-line Element (TLE) files with the Simplified General Perturbations model 4 (SGP4). However, the position error of the satellite is about 2–3 km as the orbit is predicted 2 days beyond the epoch at which the TLE file was generated (Vallado and Crawford 2008). Besides, Khalife and Kassas (2019a), Neinavaie et al. (2021) and Orabi et al. (2021) assumed that the satellite and receiver clock drifts did not change with time and lumped them into one term in the estimation. Moreover,

they ignored the ionospheric and tropospheric delay rates in the measurements due to their negligible amounts compared with the satellite velocity errors. Nevertheless, these error sources should be carefully considered in the LEO-based Doppler positioning system, or they will reduce the positioning accuracy (Psiaki 2021).

We propose a point-solution algorithm for GNSS-like navigation systems operated in LEO to analyze the error sources of Doppler positioning. LEO satellites could be modified to be equipped with navigation payloads and broadcast signals (e.g., beacon signals, short bursts) to support navigation capabilities (Reid et al. 2016; Psiaki 2021). The proposed algorithm for these LEO-based navigation systems is of great significance as they are becoming reality. In the following sections, we first describe the principle of Doppler positioning. Then, we analyze the main error sources and the Doppler positioning performance with LEO satellites. We test the sensitivity to the initial position error for the proposed algorithm and discuss the possible diversity between reality and the simulations. Finally, the conclusions are drawn.

Method and algorithm

The existing Doppler positioning methods with LEO satellites usually need to collect sufficient observations over a period of time for a static receiver (Benzerrouk et al. 2019; Tan et al. 2019; Neinavaie et al. 2021). The receiver position is calculated by multiple Doppler measurements of different satellites at different epochs. However, the researchers assumed that the satellite and receiver clock drifts were constant during the period of observation. Moreover, they used TLE files to compute the satellites' positions and ignored atmospheric delay rates in the measurements, both of which will decrease the positioning accuracy.

We propose a single-epoch least-square method for Doppler positioning with LEO satellites. Adequate Doppler measurements can be obtained in just one epoch for such a system. The proposed algorithm can simultaneously estimate the velocity, position and clock drift of the receivers, and models are used to correct for the satellite orbital errors, clock drifts and atmospheric delay rates. We introduce the Doppler dilution of precision (DDOP) to evaluate the positioning performance preliminarily.

Undifferenced Doppler positioning

The Doppler effect is caused by the relative movement between the transmitter and receiver and can be described as (Braasch and Dierendonck 1999):

$$D = f_R - f_T = \pm \frac{v_{\text{los}}}{c} \cdot f_T = \pm \frac{v_{\text{los}}}{\lambda_{f_T}} \tag{1}$$

where D is Doppler frequency shift; f_R and f_T are the received and transmitted frequencies, respectively; c is the velocity of light; λ_{f_T} is the wavelength of the transmitted signal; and v_{los} is the relative velocity magnitude between transmitter (e.g., satellite) and receiver in line-of-sight (LOS) direction. The Doppler shift is positive if the transmitter and receiver are moving toward, while it is negative if they are moving away. v_{los} is also referred to as the pseudorange rate (Braasch and Dierendonck 1999):

$$v_{los} = \left(\mathbf{v}^s - \mathbf{v}_r\right) \cdot \frac{\mathbf{p}^s - \mathbf{p}_r}{\|\mathbf{p}^s - \mathbf{p}_r\|} = \dot{\rho} \tag{2}$$

where $\mathbf{v}^s = \left[v_x^s, v_y^s, v_z^s\right]^T$ and $\mathbf{v}_r = \left[v_{r_x}, v_{r_y}, v_{r_z}\right]^T$ are the satellite and receiver velocity vectors, respectively; and $\mathbf{p}^s = \left[x^s, y^s, z^s\right]^T$ and $\mathbf{p}_r = \left[x_r, y_r, z_r\right]^T$ are the satellite and receiver position vectors, respectively; $\dot{\rho}$ is the pseudorange rate, i.e., the first derivative of pseudorange with respect to time. The pseudorange measurement equation is (Li and Huang 2013):

$$P_r^s = \|\mathbf{p}^s - \mathbf{p}_r\| + c \cdot (\delta t_r - \delta t^s) + c \cdot dR_r^s + T_r^s + I_{r,f}^s + dE_r^s + \varepsilon_p \tag{3}$$

where P_r^s is pseudorange; δt^s and δt_r are the satellite and receiver clock offsets, respectively; T_r^s and $I_{r,f}^s$ are the tropospheric and ionospheric delays, respectively; ε_p is the unmodeled errors including the observational noise and multipath error; and dR_r^s is the relativistic effect correction to satellite clock offset (Petit and Luzum 2010):

$$dR_r^s = \frac{-2}{c^2}(\mathbf{p}^s \cdot \mathbf{v}^s) \tag{4}$$

dE_r^s is the Sagnac effect term which concerns the propagation of electromagnetic signals in Earth rotating reference frame (Gulklett 2003):

$$dE_r^s = \frac{w_e}{c}\left(x^s \cdot y_r - y^s \cdot x_r\right) \tag{5}$$

where w_e is the Earth rotation angular velocity. The pseudorange rate equation is:

$$-\lambda_{f_T} \cdot D_r^s = \dot{P}_r^s = \left(\mathbf{v}^s - \mathbf{v}_r\right) \cdot \frac{\mathbf{p}^s - \mathbf{p}_r}{\|\mathbf{p}^s - \mathbf{p}_r\|} + c \cdot (\delta \dot{t}_r - \delta \dot{t}^s)$$
$$+ c \cdot d\dot{R}_r^s + \dot{T}_r^s + \dot{I}_{r,f}^s + dE_r^s + \varepsilon_{\dot{\rho}} \tag{6}$$

where $\dot{P}_r^s$ is the pseudorange rate; $\delta \dot{t}_r$ and $\delta \dot{t}^s$ are the satellite and receiver clock drifts, respectively; $\dot{T}_r^s$ and $\dot{I}_{r,f}^s$ are the

tropospheric and ionospheric delay rates, respectively; $d\dot{R}_r^s$ is the relativistic effect correction to satellite clock drift; and $d\dot{E}_r^s$ is the Sagnac effect of the range rate, which can be derived from:

$$d\dot{R}_r^s = \frac{-2}{c^2}(\dot{\mathbf{p}}^s \cdot \mathbf{v}^s + \mathbf{p}^s \cdot \dot{\mathbf{v}}^s) \tag{7}$$

$$d\dot{E}_r^s = \frac{w_e}{c}\left(v_x^s \cdot y_r + v_{r_y} \cdot x^s - v_y^s \cdot x_r - v_{r_x} \cdot y^s\right) \tag{8}$$

$\varepsilon_{\dot{\rho}}$ denotes all the unmodeled errors. The satellite velocity, position and clock drift can be obtained from the ephemeris. The linearized equation of (6) with the initial receiver value $\mathbf{X_0} = \left[x_r^0, y_r^0, z_r^0, v_{r_x}^0, v_{r_y}^0, v_{r_z}^0, \delta t_{r,0}\right]^T$ is as follows:

$$\dot{\rho}_i \approx \dot{\rho}_i^0 + \frac{\partial \dot{\rho}_i}{\partial x_r} \cdot \Delta x_r + \frac{\partial \dot{\rho}_i}{\partial y_r} \cdot \Delta y_r + \frac{\partial \dot{\rho}_i}{\partial z_r} \cdot \Delta z_r$$
$$+ \frac{\partial \dot{\rho}_i}{\partial v_{r_x}} \cdot \Delta v_{r_x} + \frac{\partial \dot{\rho}_i}{\partial v_{r_y}} \cdot \Delta v_{r_y} + \frac{\partial \dot{\rho}_i}{\partial v_{r_z}} \cdot \Delta v_{r_z} + \frac{\partial \dot{\rho}_i}{\partial \delta \dot{t}_r} \cdot \Delta \delta \dot{t}_r + \varepsilon_{\dot{\rho}_i}$$
$$\approx \dot{\rho}_i^0 + \left[\frac{\Delta v_{x_i}}{\rho_i^0} \cdot \left(e_{x_i}^2 - 1\right) + \frac{\Delta v_{y_i}}{\rho_i^0} \cdot e_{x_i} \cdot e_{y_i} + \frac{\Delta v_{z_i}}{\rho_i^0} \cdot e_{x_i} \cdot e_{z_i}\right] \cdot \Delta x_r$$
$$+ \left[\frac{\Delta v_{x_i}}{\rho_i^0} \cdot e_{y_i} \cdot e_{x_i} + \frac{\Delta v_{y_i}}{\rho_i^0} \cdot \left(e_{y_i}^2 - 1\right) + \frac{\Delta v_{z_i}}{\rho_i^0} \cdot e_{y_i} \cdot e_{z_i}\right] \cdot \Delta y_r$$
$$+ \left[\frac{\Delta v_{x_i}}{\rho_i^0} \cdot e_{z_i} \cdot e_{x_i} + \frac{\Delta v_{y_i}}{\rho_i^0} \cdot e_{z_i} \cdot e_{y_i} + \frac{\Delta v_{z_i}}{\rho_i^0} \cdot \left(e_{z_i}^2 - 1\right)\right] \cdot \Delta z_r$$
$$- e_{x_i} \cdot \Delta v_{r_x} - e_{y_i} \cdot \Delta v_{r_y} - e_{z_i} \cdot \Delta v_{r_z} + c \cdot \Delta \delta \dot{t}_r + \varepsilon_{\dot{\rho}_i} \tag{9}$$

where ρ_i^0 and $\dot{\rho}_i^0$ are the initial pseudorange and pseudorange rate, respectively; $\Delta v_{x_i} = v_x^{s,i} - v_{r_x}^0$, $\Delta v_{y_i} = v_y^{s,i} - v_{r_y}^0$ and $\Delta v_{z_i} = v_z^{s,i} - v_{r_z}^0$ are the relative velocities between the satellite and receiver; $\left[e_{x_i}, e_{y_i}, e_{z_i}\right]^T = \left[\frac{x^{s,i} - x_r^0}{\rho_i^0}, \frac{y^{s,i} - y_r^0}{\rho_i^0}, \frac{z^{s,i} - z_r^0}{\rho_i^0}\right]^T$ is the direction cosine of receiver pointing to the satellite; and $\mathbf{\Delta X}_r = \left[\Delta x_r, \Delta y_r, \Delta z_r, \Delta v_{r_x}, \Delta v_{r_y}, \Delta v_{r_z}, \Delta \delta \dot{t}_r\right]^T$ is a correction to the initial value. Combining the observations of M satellites, the least-square iteration equation and the design matrix are:

$$\mathbf{L} = \mathbf{G} \cdot \begin{bmatrix} \Delta x_r \\ \Delta y_r \\ \Delta z_r \\ \Delta v_{r_x} \\ \Delta v_{r_y} \\ \Delta v_{r_z} \\ \Delta \delta \dot{t}_r \end{bmatrix} + \begin{bmatrix} \varepsilon_{\dot{\rho}_i} \\ \varepsilon_{\dot{\rho}_j} \\ \vdots \\ \varepsilon_{\dot{\rho}_k} \end{bmatrix} = \mathbf{G} \cdot \mathbf{\Delta X}_r + \boldsymbol{\varepsilon}_{\dot{\rho}} \tag{10}$$

$$\mathbf{G} = \begin{bmatrix} \frac{\partial \dot{\rho}_1}{\partial x_r} & \frac{\partial \dot{\rho}_1}{\partial y_r} & \frac{\partial \dot{\rho}_1}{\partial z_r} & \frac{\partial \dot{\rho}_1}{\partial v_{r_x}} & \frac{\partial \dot{\rho}_1}{\partial v_{r_y}} & \frac{\partial \dot{\rho}_1}{\partial v_{r_z}} & \frac{\partial \dot{\rho}_1}{\partial \delta \dot{t}_r} \\ & & & \cdots & & & \\ \frac{\partial \dot{\rho}_i}{\partial x_r} & \frac{\partial \dot{\rho}_i}{\partial y_r} & \frac{\partial \dot{\rho}_i}{\partial z_r} & \frac{\partial \dot{\rho}_i}{\partial v_{r_x}} & \frac{\partial \dot{\rho}_i}{\partial v_{r_y}} & \frac{\partial \dot{\rho}_i}{\partial v_{r_z}} & \frac{\partial \dot{\rho}_i}{\partial \delta \dot{t}_r} \\ & & & \cdots & & & \\ \frac{\partial \dot{\rho}_m}{\partial x_r} & \frac{\partial \dot{\rho}_m}{\partial y_r} & \frac{\partial \dot{\rho}_m}{\partial z_r} & \frac{\partial \dot{\rho}_m}{\partial v_{r_x}} & \frac{\partial \dot{\rho}_m}{\partial v_{r_y}} & \frac{\partial \dot{\rho}_m}{\partial v_{r_z}} & \frac{\partial \dot{\rho}_m}{\partial \delta \dot{t}_r} \end{bmatrix}_{m \times 7} \quad (11)$$

where $\mathbf{L}$ is a column vector of observations; $\boldsymbol{\varepsilon}_{\dot{\boldsymbol{\rho}}}$ is a vector of observation noises. $\Delta \mathbf{X}_r$ is the vector of corrections and can be computed by $\Delta \mathbf{X}_r = \left(\mathbf{G}^T \cdot \mathbf{W} \cdot \mathbf{G} \right)^{-1} \mathbf{G}^T \cdot \mathbf{W} \cdot \mathbf{L}$. $\mathbf{W}$ is the weight matrix, which is usually defined as the inverse of the Doppler measurement error covariance matrix. If the Doppler errors are uncorrelated with equal variances, W is a diagonal matrix. Then, the solution is obtained by $\mathbf{X}_0 + \Delta \mathbf{X}_r$ when the iteration process converges. Using the above method, the receiver velocity, position and clock drift can be solved with at least 7 different satellites at the same time.

Doppler dilution of precision

The positioning error of standard single point positioning can be expressed as (Guan et al. 2020):

$$\sigma_{3D} = \text{GDOP} \cdot \sigma_{URE} \quad (12)$$

where σ_{URE} is the user ranging error, including clock error, atmospheric effect, etc. GDOP is the geometric dilution of precision and can reflect the positioning error caused by the geometry of visible satellites. Similarly, the relation between positioning error and DDOP is (Morales-Ferre et al. 2020):

$$\sigma_{3D,\text{Doppler}} = \text{DDOP} \cdot \sigma_{URE,\text{Doppler}} \quad (13)$$

where $\sigma_{URE,\text{Doppler}}$ is the user Doppler ranging error, which is related to the clock drift, atmospheric delay rate, etc. In the DDOP calculation, for the sake of simplicity, the identity weighting is used, i.e., the Doppler measurement weight matrix is diagonal with all the diagonal elements equal to 1. Thus, DDOP can be computed using $\text{DDOP} = \sqrt{\text{trace}[(\mathbf{G}^T \cdot \mathbf{G})^{-1}]}$. According to (13), reducing the DDOP is a way to improve the Doppler positioning

accuracy. The velocity and altitude of GNSS satellites are about 3.9 km/s and 20,200 km, respectively, making the item $\Delta v_{x_1} \cdot \left(e_{x_1} \cdot e_{x_1} - 1 \right) \big/ \rho_1$ of matrix $\mathbf{G}$ in the order of 10^{-4} and the GNSS-DDOP in the order of 10^4. For LEO satellites, the item $\Delta v_{x_1} \cdot \left(e_{x_1} \cdot e_{x_1} - 1 \right) \big/ \rho_1$ increases to 10^{-2} and the LEO-DDOP reduces to 10^2. The LEO-DDOP is less than GNSS-DDOP by 2 orders; thus, the accuracy of LEO Doppler positioning should be 100 times better than GNSS. When there are many visible satellites, one feasible way to reduce DDOP is selecting a group of satellites from all the visible satellites to improve the structure of $\mathbf{G}$ matrix and minimize DDOP.

Simulation and experiment

Since most LEO constellations are designed for communication and are still under construction, no public data are released for navigation applications. Thus, we have to simulate the ephemeris and ground observations for LEO satellites. First, we describe the data simulation and positioning processing strategies. Then we analyze the main error sources and the performance of undifferenced Doppler positioning, and discuss the possible diversity between reality and the simulations.

Data simulation and positioning processing strategies

Among all LEO constellations, Starlink is a typical heterogeneous mega-constellation consisting of different orbital shells (Cakaj 2021). An orbital shell is a walker constellation (Walker 1984); the total number of satellites, the number of orbital planes, the orbital altitude and inclination describe its geometric configuration. In order to investigate the influence of different constellations on positioning, two Starlink-like LEO constellations are simulated and their orbital shells' parameters (Zhang et al. 2022) are shown in Table 1. The 1584 satellites of Constellation A are evenly distributed on the first orbital shell. Constellation B has 4408 satellites and consists of 5 orbital shells. These satellites orbit at altitudes

Table 1 Orbital shells' parameters of Starlink-like Constellation A and B

Constellation	Shell	Total number of satellites	Number of orbital planes	Inclination (°)	Altitude (km)
A	1	1584	72	53	550
B	1	1584	72	53	550
	2	1584	72	53.2	540
	3	720	36	70	570
	4	348	6	97.6	560
	5	172	4	97.6	560

of 540–570 km. With orbital inclinations of 53°, 53.2°, 70° and 97.6°, Constellation B can guarantee global coverage.

In the simulation, the initial orbital elements of satellites are calculated according to the parameters in Table 1. Then, the satellite position and velocity at any time are propagated using orbital force models. The N-Body perturbation employs JPL DE405 (Earth, Sun, Moon, etc.) (Standish 1998). The other orbital force models include Earth gravity of degree 100 and order 100 (Reigber et al. 2005), solar radiation pressure (Ziebart 2004), DTM94 model for atmospheric density (Berger et al. 1998), tides and relativistic effects (IERS 2010 convention) (Petit and Luzum 2010). Finally, some random errors are added to simulate the orbital errors. The satellite position and velocity coordinates are simulated in the Earth-centered inertial (ECI) frame and then transformed into the Earth-centered Earth-fixed (ECEF) frame.

In early times, LEO satellites are equipped with crystal oscillators or GPS receivers to provide the frequency standard. However, their clock offsets and drifts significantly depend on the hardware. Rybak et al. (2021) recently proposed using the Clip Scale Atomic Clocks (CSACs) for small satellite navigation systems. The CSACs' clock stability at an average time of 100 min is about 10^{-12} s/s
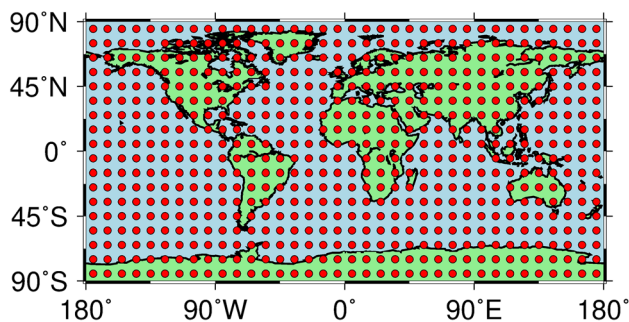

Fig. 1 Distribution of 648 stations with a spatial resolution of 10°

(Reid et al. 2016). Using the polynomial model proposed by Tavella (2008), the clock offset and drift of every LEO satellite are simulated with standard deviations of 1 us and 10^{-12} s/s, respectively.

Then, 648 stations with a spatial resolution of 10° are chosen and their distribution is shown in Fig. 1. The data simulation and positioning processing strategies are shown in Table 2. The receiver is assumed to measure a valid Doppler shift if the satellite lies above a 5° elevation angle. The C-band signal frequencies are chosen because they suffer from smaller ionospheric effects than VHF/L-band and lower attenuation (e.g., free space loss, rainfall attenuation) than Ku/Ka/V-band (Irsigler et al. 2004).

In the observation simulation, the geometric distance between the station and the satellite is first calculated. Then, the simulated Doppler observation is obtained by adding various error terms. Among them, the atmospheric delay rates are derived from the atmospheric delays by taking difference between epochs. The tropospheric delay is determined using the Saastamoninen model, the global pressure and temperature model 3 (GPT3) and the Vienna mapping functions 3 (VMF3) (Landskron and Böhm 2018). The ionospheric delay is obtained from NeQuick-G model (Aragon-Angel et al. 2019). Finally, some random errors are added to approximate the real observation. Previous studies (Neinavaie et al. 2021; Psiaki and Slosman 2019) show that the Doppler shifts can be measured precisely. Jiang et al. (2022) set the accuracy of the measured Doppler shift to be 0.1 Hz. Thus, the Doppler measurement noise is simulated by a zero-mean Gaussian distribution with a standard deviation of 0.1 Hz.

In the following sections, the receiver position and velocity are solved in ECEF coordinate and then converted into a north–east–up frame centered at the true receiver position. The root mean square (RMS) is used to evaluate the positioning accuracy.

Table 2 Data simulation and Doppler positioning processing strategies

Items	Simulation strategy	Processing strategy
Date	April 1, 2022	
Signal frequency	C-band: $f_1 = 5$ GHz, $f_2 = 7$ GHz	
Cutoff elevation angle	5°	
Satellite position and velocity	Initial orbital elements + orbital force models + random error	From ephemeris
Satellite clock drift	CSACs + polynomial model	From ephemeris
Receiver position	Stationary	Estimated as constant
Receiver clock drift	Randomly simulated with a magnitude of 10^{-6} s/s	Estimated as white noise process
Tropospheric delay rate	Saastamoninen + GPT3 + VMF3, take difference between epochs	Corrected
Ionospheric delay rate	NeQuick-G model, take difference between epochs	Corrected
Relativistic effect	(7)	Corrected
Sagnac effect	(8)	Corrected

Error analysis

LEO satellites travel at high speeds, rapidly changing their positions and elevation angles. This makes the LEO-based positioning more sensitive to satellite-related errors, i.e., the satellite position and velocity errors. Besides, the ionospheric and tropospheric delay rates become significant and should be considered in detail. Therefore, the main error sources in LEO-based Doppler positioning should be discussed.

Satellite position and velocity errors

One of the main error sources that reduce positioning accuracy is satellite position and velocity errors. The orbit determination of GNSS satellites has been widely studied, and the precision is at the centimeter level or better. However, this may be challenging for LEO satellites without onboard GNSS receivers and atomic clocks (Morales et al. 2019). Blindly using the positions of LEO satellites extrapolated by the TLE and SGP4 will reduce the positioning accuracy. The impact of satellite orbital errors in Doppler positioning should be considered in detail. In the simulation, random errors with different orders are added to the satellite position or velocity. The positioning results are shown in Table 3, where N, E and U denote north, east and up directions, respectively.

The results show that the satellite position error of several meters and velocity error of several centimeters per second will reduce the positioning accuracy. Afterward, when the satellite orbital error increases by one order of magnitude, the positioning error also increases by one order of magnitude. The 30 m per-axis position error and 30 cm/s per-axis velocity error reduce the positioning accuracy by 5.28 and 7.77 times, respectively. The 300 m position error and 3 m/s velocity error increase the positioning error by 50–77 times.

Worse still, the errors of 3 km and 30 m/s will cause about 3 km positioning errors.

Ionospheric delay rates

The ionospheric delay rate can be accessible through the first derivative of ionospheric delay with respect to time or simply taking the difference between epochs:

$$\dot{I}_{r,f}^{s}(t) = \frac{I_{r,f}^{s}(t + \Delta t) - 2I_{r,f}^{s}(t) + I_{r,f}^{s}(t - \Delta t)}{2\Delta t} \tag{14}$$

where t is the current epoch; Δt is the sampling interval; and $\dot{I}_{r,f}^{s}$ is the ionospheric delay rate. This formula actually calculates the average ionospheric delay rate over a period of time. When Δt is small enough, $\dot{I}_{r,f}^{s}$ can be considered as the instantaneous ionospheric delay rate. Since the ionospheric delay rates are related to signal frequencies and solar activities, we simulate the ionospheric delay rates of different signal frequencies under different solar activities. The simulation strategies are shown in Table 4.

The results (see Fig. 2) show that the ionospheric delay rates in high solar activity are the largest, while medium and low solar activities follow. The ionospheric delay rates of LEO satellites (350–2000 km altitudes) are much greater than that of satellites at 5000–30,000 km altitudes. Thus, the ionospheric delay rates of LEO satellites should be discussed in detail. Take Orbcomm satellites (825 km altitude and VHF-band) as an example, its ionospheric delay rate ranges from 9 to 29 m/s under different solar activities. If the LEO satellites broadcast signals in L-band, there will be 3–21 cm/s ionospheric delay rates, which will cause 6–42 m errors in Doppler positioning. These indicate that the VHF/L-band signals ionospheric delay rates cannot be neglected in LEO positioning. The ionospheric delay rate is inversely proportional to the square of the frequency. Thus, the higher the frequency, the lower the ionospheric delay

Table 3 Doppler positioning accuracy with different orbital errors

Satellite position error (m)	Satellite velocity error (cm/s)	RMS-N (m)	RMS-E (m)	RMS-U (m)	RMS-3D (m)
0.0	0.0	1.379	2.920	4.070	5.195
0.03	0	1.378	2.921	4.070	5.196
0	0.3	1.384	2.950	4.091	5.230
3	0	1.602	3.516	4.364	5.829
0	3	1.749	3.934	5.109	6.681
30	0	8.196	18.776	18.261	27.444
0	30	10.953	25.828	29.017	40.361
300	0	80.279	178.167	183.805	268.277
0	300	108.827	255.685	286.723	399.285
3000	0	790.073	1865.394	1773.159	2692.212
0	3000	1085.340	2561.022	2842.690	3977.145

Table 4 Ionospheric delay rate simulation strategies

Items	Strategy
Date	April 1
Solar activity coefficients (a_{i0}, a_{i1}, a_{i2})	High (236.831641, -0.393629, 0.004028) Medium (121.129893, 0.351254, 0.013464) Low (2.580271, 0.127628, 0.025275)
Satellite orbital altitude	350, 400, 450, 500, 550, 1000, 2000, 5000, 10,000, 20,000, 30,000 km
Station	Static, BLH = (358.72°, 16.25°, 78.11 m)
Signal frequency	123 MHz, 1.5 GHz, 5 GHz, 15 GHz, 20 GHz, 35 GHz
Ionospheric delay	NeQuick-G model
Ionospheric delay rate	Take difference between epochs, $\Delta t = 0.1$ s

Fig. 2 Ionospheric delay rates of different signals under different solar activities and orbital attitudes
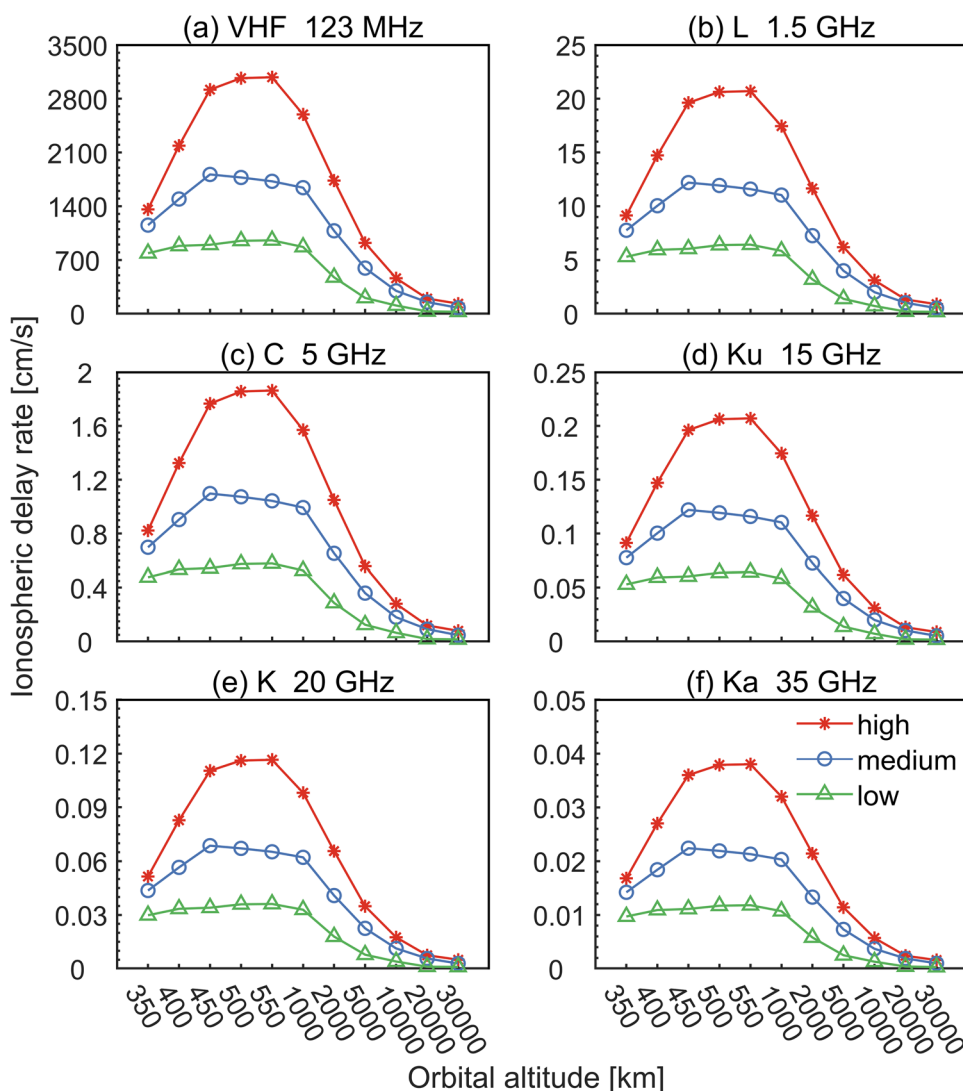
rate. If the C-band signal is used for LEO navigation, there will be 0.3–2 cm/s ionospheric delay rates, which will cause 0.6–4 m errors in Doppler positioning. For Ka/K/Ku-band signals, their ionospheric delay rates are less than 0.21 cm/s.

Then, we add the C-band signal ionospheric delay rates into the observation simulations. The results in Fig. 3a

and b show that there will be errors in all directions if the ionospheric errors are not corrected. The 3D RMS of positioning results in Fig. 3a is 1 m, and the 3D RMS of positioning results in Fig. 3b is 2.1 m. This is consistent with the above theoretical value in Fig. 2. For dual-frequency receivers, the ionospheric delay rate can be eliminated using

Fig. 3 Doppler positioning errors caused by C-band signal ionospheric delay rates (without orbital errors); three rows represent the positioning accuracy for N, E and U directions, respectively
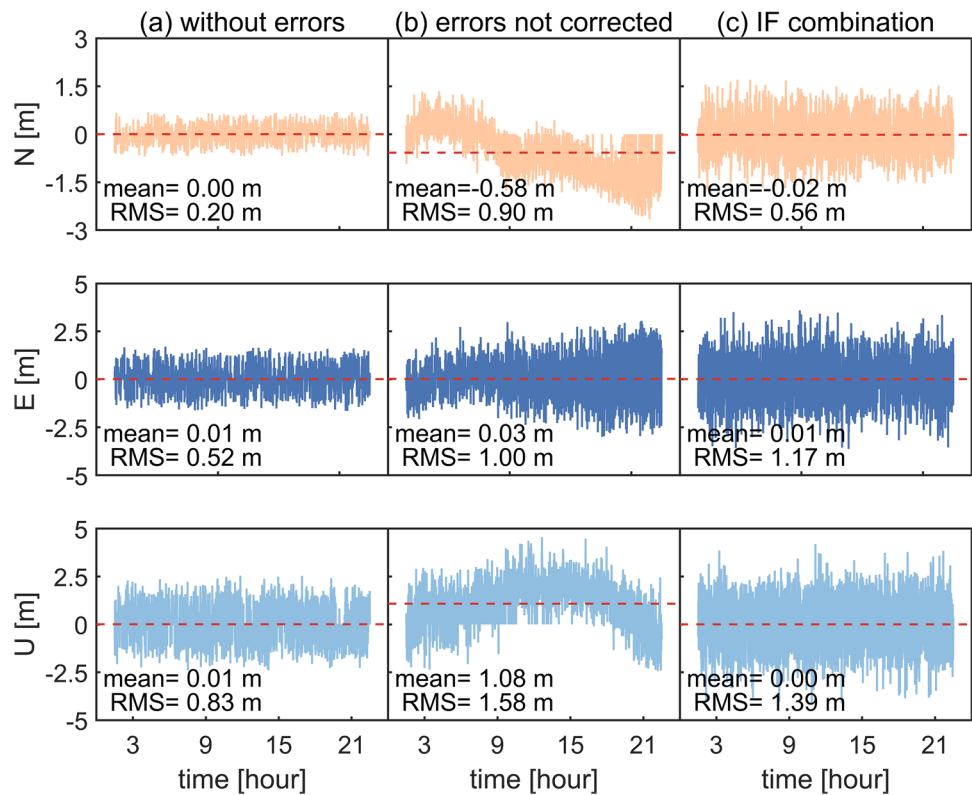
the ionosphere-free (IF) combination of pseudorange rate measurements:

$$\dot{P}_{IF} = \frac{f_1^2}{f_1^2 - f_2^2} \cdot \dot{P}_1 - \frac{f_2^2}{f_1^2 - f_2^2} \cdot \dot{P}_2 \qquad (15)$$

where $\dot{P}_1$ and $\dot{P}_2$ are pseudorange rates at f_1 and f_2, respectively. The 3D RMS of positioning errors for the IF combination (in Fig. 3c) is about 1.9 m. This is about 2 times as large as the results in Fig. 3a. The reason is that IF combination amplifies the measurement noise (0.1 Hz) and influences the positioning performance (Bolla and Borre 2019; Collins 1999; Zhang et al. 2010).

Tropospheric delay rates

In the simulation, the tropospheric delay rates are derived by taking the difference between epochs. The sampling interval is also set to be 0.1 s. The tropospheric delays are calculated using the Saastamoninen model, GPT3 meteorological parameters and VMF3 mapping function. Among them, the mapping function is related to the elevation angle. The time, station and orbital altitude are the same as the ionospheric delay rates simulation strategies shown in Table 4.

The results of tropospheric delay rates with different satellite orbital altitudes are shown in Fig. 4. For LEO satellites with altitudes of 350–550 km, the tropospheric
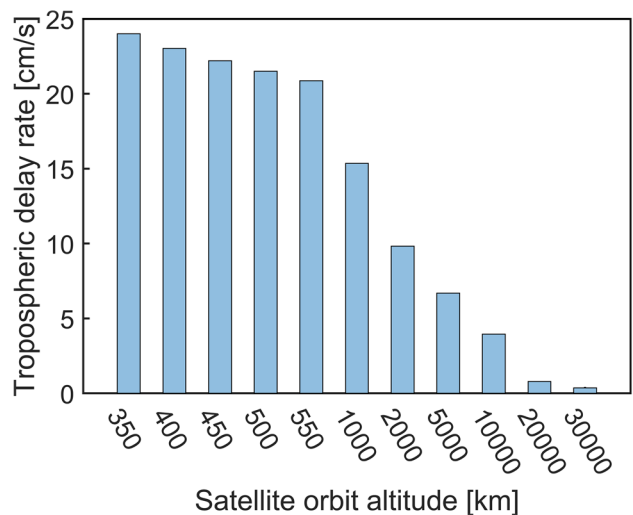

Fig. 4 Tropospheric delay rates with different satellite orbital altitudes

delay rates are 21–25 cm/s, which, if not corrected, will cause 42–50 m errors in Doppler positioning. As for GNSS satellites with altitudes of about 20,000 km, the tropospheric delay rate is decreased sharply to 1 cm/s. The tropospheric delay rates with satellite altitudes below 1000 km are far greater than those above 2000 km. This

phenomenon may be caused by the rapid change of elevation angles when LEO satellites travel at high speeds.

Then, the tropospheric errors are added to the observation simulations. The tropospheric delay rates are derived by taking the difference between the tropospheric delays at different epochs. The tropospheric delays along the signal paths are obtained through the simulated zenith total delay (ZTD) with the VMF3 mapping function. The ZTD is calculated by adding the zenith hydrostatic delay (ZHD) into zenith wet delay (ZWD), which are obtained using the Saastamoninen model and GPT3 meteorological parameters. The positioning results of 21 stations with (red bars) or without (yellow bars) tropospheric errors are shown in Fig. 5. These stations are composed of three evenly selected stations at 7 lines of latitude (45W, 30W, 15W, 0, 15N, 30N and 45N). The blue bars are the positioning results after corrections using the Saastamoninen model and its mapping function (which differs from VMF3). The red bars in Fig. 5 show that the positioning accuracy will sharply deteriorate without corrections for the tropospheric errors. The positioning errors in U direction are increased by 20–60 m. This is consistent with the above theoretical value in Fig. 4. The positioning results after corrections (blue bars in Fig. 5) show

a bit different from the results without tropospheric errors (yellow bars in Fig. 5). This probably is because the mapping functions we used in the observation simulation and positioning process is different.

Undifferenced Doppler positioning performance

The data simulation and positioning processing strategies are shown in Table 2. The undifferenced Doppler positioning RMS and DDOP are shown in Figs. 6 and 7. The RMSs and DDOPs of stations in mid latitude zones are the smallest, followed by the low- and high-latitude zones. This phenomenon is thought to be related to the constellation configuration (Reid et al. 2018; Zhang et al. 2022). Then, we calculate the average RMSs of global stations. The average RMSs in N, E and U directions are 1.48, 2.73 and 2.83 m with Constellation A and 0.89, 1.53 and 2.19 m with Constellation B. The positioning accuracy is at the meter level which is comparable to the pseudorange-based positioning in GNSS.

Besides, the results show that the spatial distribution of DDOPs are consistent with the RMSs. We calculate the correlation between DDOPs and U-RMSs of stations in the 5°N latitudinal zone. The correlation coefficient is 0.907 (Fig. 8).

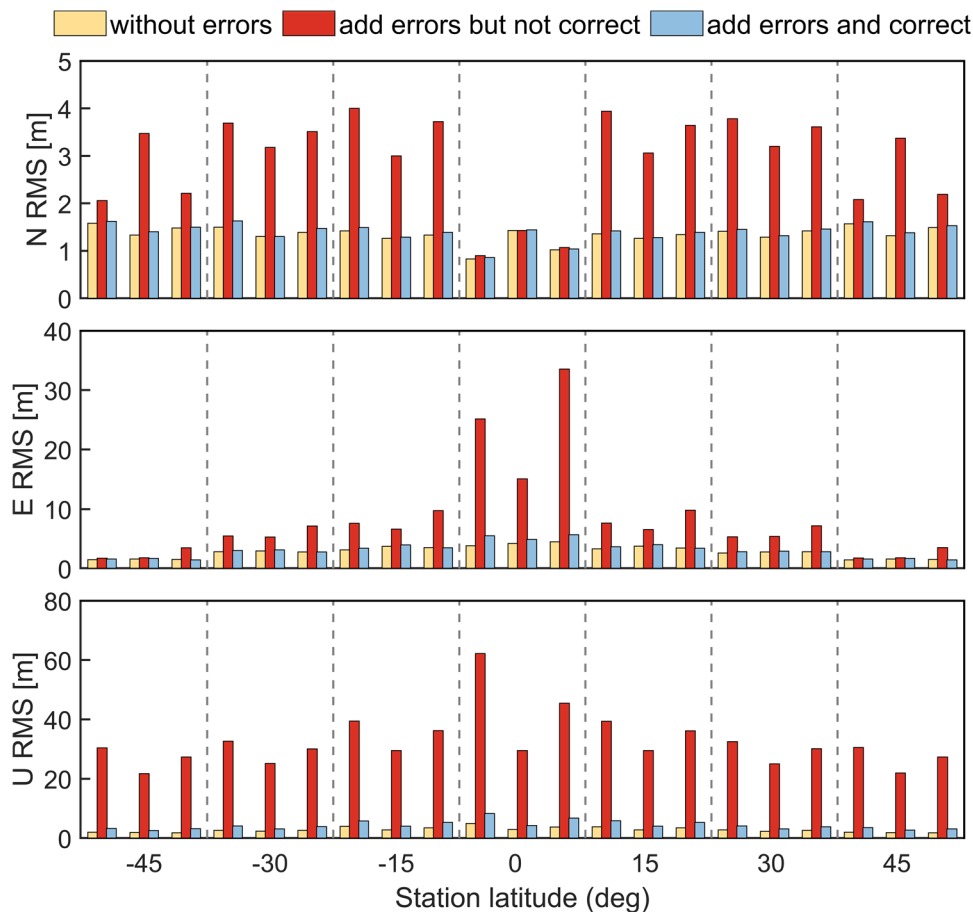**Fig. 5** Doppler positioning errors caused by tropospheric errors (without orbital errors)

Fig. 6 Undifferenced Doppler positioning results with Constellation A (left) and Constellation B (right). The white-colored zones indicate that there are no solutions for these stations
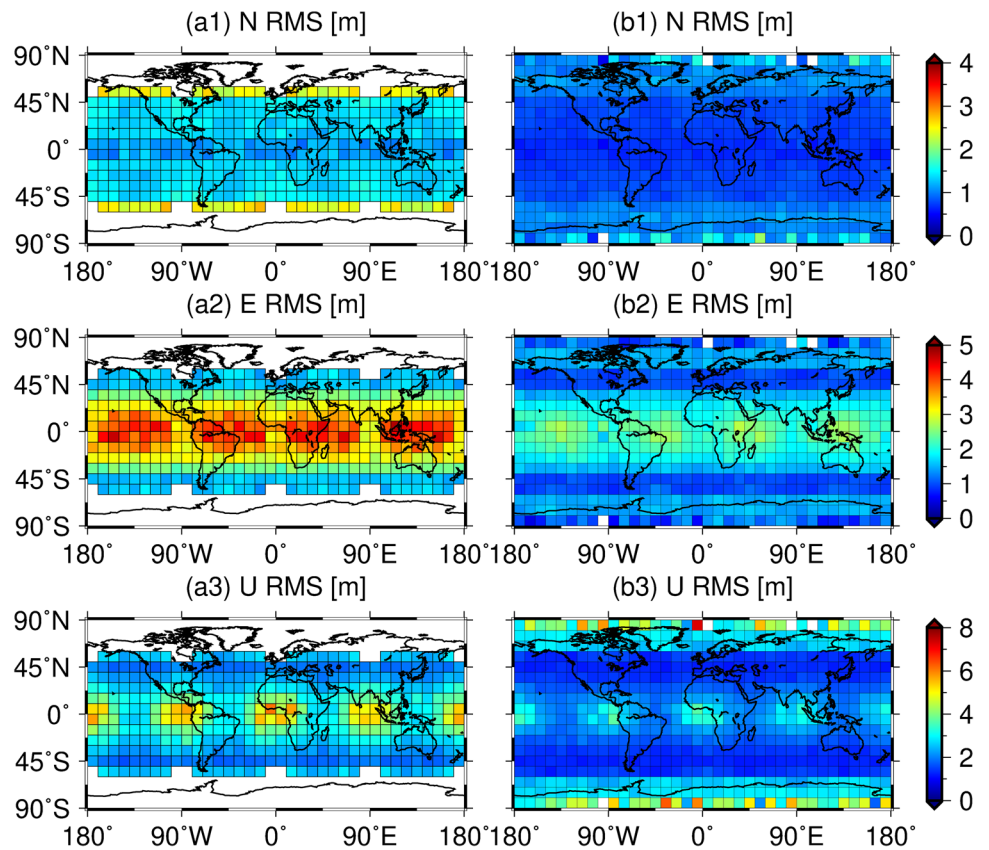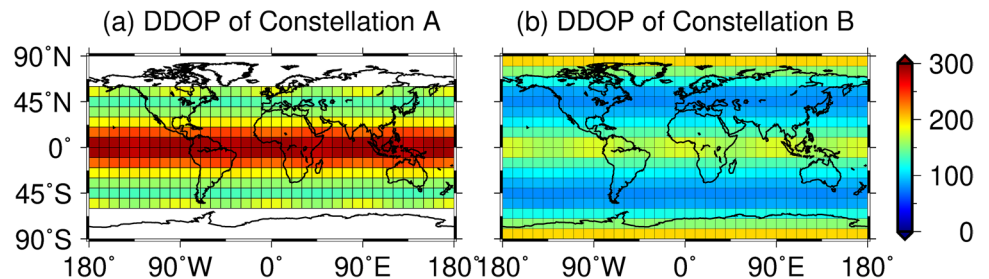
(a1) N RMS [m]   (b1) N RMS [m]

(a2) E RMS [m]   (b2) E RMS [m]

(a3) U RMS [m]   (b3) U RMS [m]

Fig. 7 DDOPs of global stations with Constellation A (**a**) and Constellation B (**b**)

(a) DDOP of Constellation A   (b) DDOP of Constellation B

This indicates that the DDOP can reflect the positioning accuracy of undifferenced Doppler positioning.

Sensitivity of initial position error

The nonlinear least-square method needs an appropriate initial position value to ensure convergence. In GNSS, even if the initial receiver position value is set to be 0, the solution can still converge. However, the situation is different with LEO satellites due to their low orbital altitudes. Thus, the LEO-based Doppler positioning algorithm should be tested for its sensitivity to initial position error. The actual receiver position is (6,123,320.353, −136,480.099, 1,773,905.419) km in ECEF. The initial errors are added
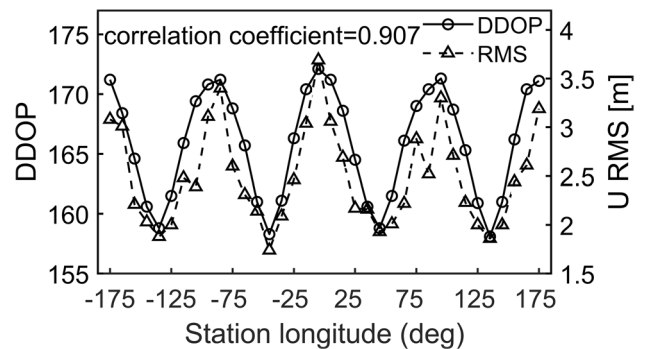
Fig. 8 DDOPs and U-RMSs of stations in the 5° N latitudinal zone

Table 5 Positioning results with different initial receiver position errors

Initial error (km)	RMS-N (m)	RMS-E (m)	RMS-U (m)	Solution epochs
0	2.451	0.449	1.488	2521
10	2.451	0.449	1.488	2521
100	2.451	0.449	1.488	2521
300	2.452	0.448	1.489	2511
350	2.446	0.449	1.477	1824
400	2.507	0.378	1.548	82
405	2.509	0.538	1.716	5
410	No solution			
450	No solution			

in all directions. The simulation time is from 1:30 to 22:30 with an interval of 30 s. Thus, there are 2521 epochs in total. The positioning results with different initial position errors are shown in Table 5.

The results show that with an initial position error of 300 km or larger, the iteration process may be divergent. With an initial error of 410 km, the iterative algorithm cannot converge to the actual position, resulting in no solution. These indicate that the LEO-based Doppler positioning is sensitive to the initial position error. The initialization of the receiver position should be paid more attention and an appropriate initial position value must be given in LEO-based Doppler positioning.

Diversity between reality and the simulations

We examine the performance of the proposed methods on simulated data. The possible diversity between reality and the simulations must be discussed in detail to make the proposed methods work in practice.

First, the proposed methods assume that the receiver can see many LEO satellites simultaneously. Generally, the number of visible satellites from one earlier constellation (e.g., Iridium, Orbcomm) is 1–2 for communication purposes. In recent years, the rapidly developed broadband mega-constellations have enabled many satellites to be visible. Among them, the Starlink already has over 3200 satellites in orbit by February 2023 (https://satellitemap.space/?constellation=starlink). Neinavaie et al. (2021) explored the first Doppler tracking and positioning results with six real Starlink LEO satellites over a period of 800 s. In the near future, more than 7 satellites could be visible at the same time with these broadband LEO constellations.

In the simulation, we assumed that the satellite positions could be determined with an error of several meters. In fact, this can be achieved with a GNSS receiver onboard the LEO satellites (Reid et al. 2018). Furthermore, if the real-time

precise positions for the GNSS satellites are provided, the position errors of LEO satellites could be in several centimeters (Montenbruck et al. 2005). The satellite clock offset and drift are simulated with standard deviations of 1 us and 10^{-12} s/s, respectively. This can be easily achieved for LEO satellites with onboard GNSS receivers and CSACs, which has been used for small satellite navigation systems (Reid et al. 2016; Rybak et al 2021).

It must be noted that a mismatch may exist between the true atmospheric effects and the models used in the simulation. However, little is known about the influence of tropospheric or ionospheric modeling errors on Doppler measurements of LEO satellites. Graziani et al. (2009) estimated and corrected the tropospheric effect on Doppler shift for deep space probe navigation purposes. Their results showed that the residual uncalibrated tropospheric and/or antenna mechanical noise dominated the range rate residuals. Our simulation results also showed that the Doppler positioning accuracy would be reduced by dozens of meters if there are no corrections for tropospheric delay rates. The accuracy of tropospheric delays estimation using the precise point positioning (PPP) method with LEO-enhanced GNSS (LeGNSS) observations can be at the millimeter level, although this result is based on simulation and not for the tropospheric delay rates (Zhang et al. 2023). This provides evidence that the tropospheric delay rates of LEO satellites can also be estimated and corrected precisely.

Klobuchar (1996) briefly discussed the ionospheric effects on the Doppler shift and pointed out that the ionosphere could change rapidly by at least one order of magnitude each day. Since most LEO satellites operate within the ionosphere, the classic thin-shell ionospheric model cannot correct ionospheric errors. The NeQuick model, the altimetry data from the JASON/TOPEX satellite and the occultation data from COSMIC may be suitable for LEO satellites (Li et al. 2018; Wang et al. 2017; Yao et al. 2018). Li et al. (2022) proposed a regional bottom-side ionospheric map (RBIM) using the LEO navigation augmentation signals and validated their product based on the NeQuick-G model. Our simulation results based on the NeQuick-G model showed that the ionospheric delay rates of Ka/K/Ku-band signals are less than 0.21 cm/s. This means that the ionospheric delay rates are negligible for the Ku-band Starlink signals and can be removed from the Doppler data.

Conclusion

We propose a point-solution algorithm for a GNSS-like navigation system operated in LEO based on the assumption that LEO satellites could be modified to support navigation capabilities. The proposed algorithm can estimate the state

of the receiver solely using Doppler shifts. Then, we discuss the main error sources in LEO-based Doppler positioning. As one of the main error sources, the satellite position and velocity errors should be within several meters and several centimeters per second, respectively, to ensure meter-level positioning accuracy. Otherwise, the positioning results will sharply deteriorate. The ionospheric and tropospheric delay rates for LEO satellites are far greater than that for GNSS satellites due to the rapid change of LEO satellites' positions. The positioning accuracy will deteriorate sharply by dozens of meters if there are no corrections for the atmospheric errors. Subsequently, we analyze the performance of LEO-based Doppler positioning. The accuracy of undifferenced Doppler positioning is at meter level with a global average RMS better than 3 m. Afterward, the LEO-based Doppler positioning method is tested for its sensitivity to the initial receiver position value. If the initial position error exceeds 300 km, the solution may diverge terribly from the actual position. Thus, an appropriate initialization must be provided to ensure convergence.

Owing to the fact that there are sufficient visible satellites with LEO constellations, the satellite selection algorithm will be developed to improve positioning accuracy. Besides, given the encouraging results shown in this study, additional work should focus on designing the navigation payloads and signals to enable LEO satellites to support navigation capabilities.

Author contributions   All authors contributed to the conception and design of the study. Material preparation, data collection and analysis were performed by CS, YZ and ZL. The first draft of the manuscript was written by YZ, and all authors commented on previous versions of the manuscript. All authors read and approved the final manuscript.

Data availability   All ephemeris and observations used in this study are simulated. The Starlink orbital parameters are obtained from the SpaceX non-geostationary satellite system Attachment A: technical information to supplement Schedule S (https://www.fcc.report/IBFS/SAT-MOD-20181108-00083/1569860.pdf.) and verified using TLE files and SGP4 model (https://celestrak.org/norad/elements/table.php?GROUP=starlink&FORMAT=tle) in our early work (Zhang et al. 2022). The a_{i0}, a_{i1} and a_{i2} coefficients used in NeQuick-G model are obtained from the Galileo navigation broadcast message.

Declarations

Competing interests   The authors declare no competing interests.

References

Anderle RJ (1979) Accuracy of geodetic solutions based on Doppler measurements of the Navstar global positioning system satellites. Bull Géod 53(2):109–116

Aragon-Angel A, Zürn M, Rovira-Garcia A (2019) Galileo ionospheric correction algorithm: an optimization study of NeQuick-G. Radio Sci 54(11):1156–1169

Ardito CT, Morales JJ, Khalife JJ, Abdallah A, Kassas ZM (2019) Performance evaluation of navigation using LEO satellite signals with periodically transmitted satellite positions. In: Proc ION ITM 2019, Institute of Navigation, Reston, Virginia, USA, January 28–31, 306–318

Benzerrouk H, Nguyen Q, Fang X, Amrhar A, Rasaee H, Landry RJ (2019) LEO satellites based Doppler positioning using distributed nonlinear estimation. IFAC-PapersOnLine 52(12):496–501

Berger C, Biancale R, Ill M, Barlier F (1998) Improvement of the empirical thermospheric model DTM: DTM94: a comparative review of various temporal variations and prospects in space geodesy applications. J Geod 72:161–178

Bolla P, Borre K (2019) Performance analysis of dual-frequency receiver using combinations of GPS L1, L5, and L2 civil signals. J Geod 93:437–447

Braasch MS, Dierendonck AJ (1999) GPS receiver architectures and measurements. Proc IEEE 87(1):48–64

Cakaj S (2021) The parameters comparison of the "Starlink" LEO satellites constellation for different orbital shells. Front Comms Net 2:1–15

Chen X, Gao W, Wan Y (2013) Revisiting the Doppler filter of LEO satellite GNSS receivers for precise velocity estimation. J Electron 30(2):138–144

Collins JP (1999) An overview of GPS inter-frequency carrier phase combinations. Techn Memo 18:1–15

Farhangian F, Landry R (2020) Multi-constellation software-defined receiver for Doppler positioning with LEO satellites. Sensors 20(20):5866–5883

Graziani A, Bertacin R, Tortora P, Schiavone A, Mercolino M, Budnik F (2009) A GPS based Earth troposphere calibration system for Doppler tracking of deep space probes. In: Proc ION GNSS 2009, Institute of Navigation, Savannah, GA, September 22–25, 2575–2583

Guan M, Xu T, Gao F, Nie W, Yang H (2020) Optimal walker constellation design of LEO-based global navigation and augmentation system. Remote Sens 12(11):1845

Gulklett M (2003) Relativistic effects in GPS and LEO. University of Copenhagen, Department of Geophysics, The Niels Bohr Institute, Denmark

Irsigler M, Hein GW, Schmitz-Peiffer A (2004) Use of C-Band frequencies for satellite navigation: benefits and drawbacks. GPS Solut 8(3):119–139

Jayles C, Chauveau JP, Rozo F (2010) DORIS/Jason-2: better than 10 cm on-board orbits available for near-real-time altimetry. Adv Space Res 46(12):1497–1512

Jiang M, Qin H, Zhao C, Sun G (2022) LEO Doppler-aided GNSS position estimation. GPS Solut 26:31

Joerger M, Gratton L, Pervan B, Cohen CE (2010) Analysis of Iridium-augmented GPS for floating carrier phase positioning. Navigation 57(2):137–160

Kershner R, Newton R (1962) The transit system. J Navig 15(2):129–144

Khalife JJ, Kassas ZM (2019a) Receiver design for Doppler positioning with LEO satellites. In: 2019a IEEE international conference on acoustics, speech and signal processing (ICASSP), Brighton, UK, May 12–17, 5506–5510

Khalife JJ, Kassas ZM (2019b) Assessment of differential carrier phase measurements from Orbcomm LEO satellite signals for opportunistic navigation. In: Proc ION GNSS+ 2019b, Institute of Navigation, Miami, Florida, USA, September 16–20, 4053–4063

Khalife JJ, Neinavaie M, Kassas ZM (2020) Navigation with differential carrier phase measurements from megaconstellation LEO satellites. In: Proc IEEE/ION PLANS 2020, Institute of Navigation, Portland, OR, USA, April 20–23, 1393–1404

Khalife JJ, Neinavaie M, Kassas ZM (2021) Blind Doppler tracking from OFDM signals transmitted by broadband LEO satellites. In: 2021 IEEE 93rd vehicular technology conference (VTC2021-Spring). IEEE, Helsinki, Finland, April 25–28, 1–5

Klobuchar JA (1996) Ionosphere effects of GPS. In: Parkinson B, Spilker JJ (Eds.) Global positioning system: theory and applications, Volume 1, pp 485–515

Kouba J (1983) A review of geodetic and geodynamic satellite Doppler positioning. Rev Geophys 21(1):27–40

Landskron D, Böhm J (2018) VMF3/GPT3: refined discrete and empirical troposphere mapping function. J Geod 92(4):349–360

Lawrence D, Cobb HS, Gutt G, Tremblay F, Laplante P, O'Connor M (2016) Test results from a LEO-satellite-based assured time and location solution. In: Proc ION GNSS+ 2016, Institute of Navigation, Monterey, California, USA, January 25–28, 125–129

Li Z, Huang J (2013) GPS surveying and data processing. Wuhan University Press, Wuhan

Li M, Yuan Y, Wang N, Li Z, Huo X (2018) Performance of various predicted GNSS global ionospheric maps relative to GPS and JASON TEC data. GPS Solut 22:55

Li X, Ma F, Li X, Lv H, Bian L, Jiang Z, Zhang X (2019) LEO constellation-augmented multi-GNSS for rapid PPP convergence. J Geod 93(5):749–764

Li T, Wang L, Fu W, Han Y, Zhou H, Chen R (2022) Bottomside ionospheric snapshot modeling using the LEO navigation augmentation signal from the Luojia-1A satellite. GPS Solut 26:6

Meng Y, Bian L, Han L, Lei W, Yan T, He M, Li X (2018) A global navigation augmentation system based on LEO communication constellation. In: Proceedings of the 2018 European Navigation Conference (ENC), Gothenburg, Sweden, May 14–17, 65–71

Montenbruck O, Van Helleputte T, Kroes R, Gill E (2005) Reduced dynamic orbit determination using GPS code and carrier measurements. Aerosp Sci Technol 9(3):261–271

Morales JJ, Khalife JJ, Cruz US, Kassas ZM (2019) Orbit modeling for simultaneous tracking and navigation using LEO satellite signals. In: Proc ION GNSS+ 2019, Institute of Navigation, Miami, Florida, USA, September 16–20, 2090–2099

Morales-Ferre R, Lohan ES, Falco G, Falletti E (2020) GDOP-based analysis of suitability of LEO constellations for future satellite-based positioning. In: Proc of the 2020 IEEE International Conference on Wireless for Space and Extreme Environments (WiSEE), Vicenza, Italy, October 12–14, 147–152

Neinavaie M, Khalife JJ, Kassas ZM (2021) Acquisition, Doppler tracking, and positioning with Starlink LEO satellites: first results. IEEE Trans Aerosp Electron Syst 58(3):2606–2610

Orabi M, Khalife JJ, Kassas ZM (2021) Opportunistic navigation with Doppler measurements from Iridium Next and Orbcomm LEO satellites. In: 2021 IEEE Aerospace Conference, IEEE, Big Sky, MT, USA, March 06–13, 1–9

Park B, Jeon S, Kee C (2011) A closed-form method for the attitude determination using GNSS Doppler measurements. Int J Control Autom Syst 9(4):701–708

Petit G, Luzum B (2010) IERS Conventions (2010). IERS technical note, vol 36. Verlag des Bundesamts für Kartographie und Geodäsie, Frankfurt am Main, Germany

Psiaki ML (2021) Navigation using carrier Doppler shift from a LEO constellation: transit on steroids. Navigation 68(3):621–641

Psiaki ML, Slosman BD (2019) Tracking of digital FM OFDM Signals for the determination of navigation observables. In: Proc. ION GNSS+ 2019, Institute of Navigation, Miami, Florida, USA, September 16–20, 2325–2348

Reid TG, Neish AM, Walter T, Enge PK (2018) Broadband LEO constellations for navigation. Navigation 65(2):205–220

Reid TG, Neish AM, Walter TF, Enge PK (2016) Leveraging commercial broadband LEO constellations for navigating. Proc. ION GNSS+ 2016, Institute of Navigation, Portland, Oregon, USA, September 12–16, 2300–2314

Reigber C, Schmidt R, Flechtner F, König R, Meyer U, Neumayer KH, Schwintzer P, Zhu SY (2005) An earth gravity field model complete to degree and order 150 from GRACE: EIGEN-GRACE02S. J Geodyn 39(1):1–10

Rybak MM, Axelrad P, Seubert J, Ely T (2021) Chip scale atomic clock-driven one-way radiometric tracking for low-earth-orbit cubesat navigation. J Spacecraft Rockets 58(1):200–209

Standish EM (1998) JPL planetary and lunar ephemerides, DE405/LE405. JPL Interoffice Memorandum IOM 312. F-98-048

Tan Z, Qin H, Cong L, Zhao C (2019) Positioning using IRIDIUM satellite signals of opportunity in weak signal environment. Electronics 9(1):37

Tavella P (2008) Statistical and mathematical tools for atomic clocks. Metrologia 45(6):183–192

Vallado D, Crawford P (2008) SGP4 orbit determination. In: Proceedings of AIAA/AAS astrodynamics specialist conference and exhibit, Honolulu, Hawaii, August 18–21, pp 6770

Walker JG (1984) Satellite constellations. J Br Interplanet Soc 37(12):559–571

Wang N, Yuan Y, Li Z, Li Y, Huo X, Li M (2017) An examination of the Galileo NeQuick model: comparison with GPS and JASON TEC. GPS Solut 21:605–615

Yao Y, Liu L, Kong J, Zhai C (2018) Global ionospheric modeling based on multi-GNSS, satellite altimetry, and formosat-3/COSMIC data. GPS Solut 22:104

Zeng T, Sui L, Jia X, Lv Z, Ji G, Dai Q, Zhang Q (2018) Validation of enhanced orbit determination for GPS satellites with LEO GPS data considering multi ground station networks. Adv Space Res 63(9):2938–2951

Zhang B, Ou J, Yuan Y, Zhong S (2010) Precise point positioning algorithm based on original dual-frequency GPS code and carrier-phase observations and its application. Acta Geod Cartogr Sin 39(5):478–483

Zhang P, Ding W, Qu X, Yuan Y (2023) Simulation analysis of LEO constellation augmented GNSS (LeGNSS) zenith troposphere delay and gradients estimation. IEEE Trans Geosci Remote Sens 61:1–12

Zhang Y, Li Z, Shi C, Fang X (2022) Analysis of positioning performance and GDOP based on Starlink LEO constellation. In: Proceedings of the China Satellite Navigation Conference (CSNC) 2022, Beijing, China, May 25, 47–55

Zhao Q, Wang C, Guo J, Yang G, Liao M, Ma H, Liu J (2017) Enhanced orbit determination for BeiDou satellites with Feng-Yun-3C onboard GNSS data. GPS Solut 21(3):1179–1190

Ziebart M (2004) Generalized analytical solar radiation pressure modeling algorithm for spacecraft of complex shape. J Spacecr Rockets 41(5):840–848

Chuang Shi is currently a Professor at the School of Electronic and Information Engineering at Beihang University, China. He has over 30 years of research experience in the theory and applications of space-based PNT technology and authored 230 research papers and over 30 patents. His research interests include network adjustment and precise orbit determination of GNSS satellites and LEOs.

Zhen Li holds a Ph.D. in astrodynamics and space geodesy. He works at Beihang University as an assistant professor. His research interests include nonconservative force modeling for spacecraft with very complex shapes, space-based positioning technology and space object identification. He is now working on the development of positioning techniques using megaconstellations from Low Earth Orbit.

Yulu Zhang is pursuing her master's degree at the School of Electronic and Information Engineering at Beihang University. She works at the Laboratory of Navigation and Communication Fusion Technology, Ministry of Industry and Information Technology of China. Her current research interests include positioning and navigation with LEO satellites, precise positioning technology and the Doppler positioning algorithm.